J. Fluid Mech. (1985), *vol.* 157, *pp.* 375–404
Printed in Great Britain

A separated-flow model for collapsible-tube oscillations

By CLAUDIO CANCELLI

Dipartimento di Ingegneria Aeronautica e Spaziale, Politecnico di Torino, Corso Duca degli Abruzzi 24, 10129 Torino, Italy

AND T. J. PEDLEY

Department of Applied Mathematics and Theoretical Physics, Silver Street, Cambridge CB3 9EW, England

(Received 3 January 1984 and in revised form 27 February 1985)

A new model is presented to describe flow in segments of collapsible tube mounted between two rigid tubes and surrounded by a pressurized container. The new features of the model are the inclusion of (*a*) longitudinal wall tension and (*b*) energy loss in the separated flow downstream of the time-dependent constriction in a collapsing tube, in a manner which is consistent with the one-dimensional equations of motion. As well as accurately simulating steady-state collapse, the model predicts self-excited oscillations whose amplitude is large enough to be observable only if the flow in the collapsible tube becomes supercritical somewhere (fluid speed exceeding long-wave propagation speed). The dynamics of the oscillations is dominated by longitudinal movement of the point of flow separation, in response to the adverse pressure gradient associated with waves propagating backwards and forwards between the (moving) narrowest point of the constriction and the tube outlet.

1. Introduction

Virtually all fluid-carrying conduits in the body have elastic walls and can collapse if subjected to a sufficiently negative transmural (internal minus external) pressure. Examples include blood vessels, bronchial airways, the urethra, the gut (Shapiro 1977*a*). When fluid flows along such a tube, even the frictional pressure drop can be enough to trigger collapse. There have been a large number of laboratory experiments, using rubber tubes, designed to investigate such flow-induced collapse, and a typical experiment is depicted in figure 1. A length of collapsible tube is mounted horizontally between two rigid tubes, to which it is clamped, and is surrounded by a chamber in which the pressure can be independently adjusted (this arrangement is often called a 'Starling resistor'). Incompressible fluid flows along the tube from a constant-head reservoir, and the flow rate can be controlled by adjusting the resistances of the rigid parts of the system upstream and downstream of the collapsible segment. The Reynolds number is commonly in the range 500–5000. Two principal results have in general been obtained from these experiments. (i) Above a critical value, the flow rate depends on the difference between upstream pressure and chamber pressure and is independent of the pressure and resistance downstream of the collapsible segment ('flow limitation'). (ii) Even in experiments designed to investigate steady pressure–flow relationships, unsteady flow has commonly been observed: large-amplitude self-excited oscillations develop in the tube cross-sectional area and the outflow

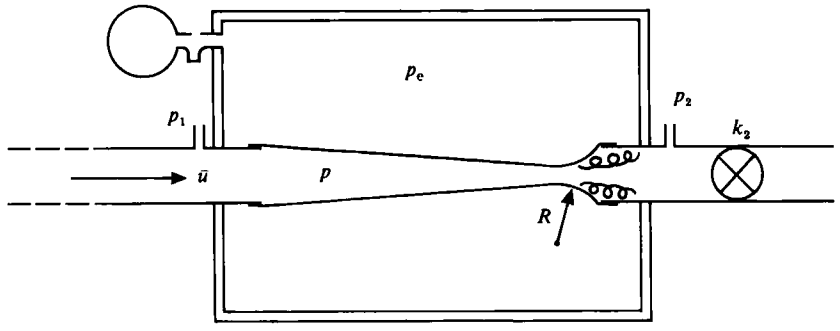

FIGURE 1. Sketch of a conventional collapsible-tube experiment, showing separated flow at the constriction; k_2 represents a downstream control valve; R is a radius of curvature of the longitudinal section.

velocity for a range of values of the governing parameters (Conrad 1969; Katz, Chen & Moreno 1969; Ur & Gordon 1970; Griffiths 1977; Brower & Scholten 1975; Bonis & Ribreau 1978; Lyon *et al.* 1981; Bertram 1982). It is thought that such oscillations may be responsible for the Korotkoff sounds heard when the brachial artery is compressed by a blood-pressure-measuring cuff (Ur & Gordon 1970; Pedley 1980; Conrad, McQueen & Yellin 1980).

There have been several attempts to explain theoretically the self-excited oscillations, and these can be divided into two groups. One group can be classified as lumped-parameter models, in which the geometry of the collapsible segment is represented by one or two time-dependent variables such as the cross-sectional area A_N at the narrowest point, and the elastic properties are represented by a single-valued relationship between A_N and the transmural pressure at the narrowest point. Conservation of fluid mass and momentum or energy are represented by integral forms of the governing equations. Such models do predict self-excited oscillations in certain circumstances, and serve to emphasize the important constraints exerted on such oscillations by the mechanical properties of the upstream and downstream rigid segments (Conrad 1969; Katz *et al.* 1969; Schoendorfer & Shapiro 1977; Conrad, Cohen & McQueen 1978; Cancelli & Chiocchia 1979; Pedley 1980; Bertram & Pedley 1982). An important factor in the predicted oscillations, emphasized particularly by Bertram & Pedley (1982), is the amount of energy lost in the flow emerging as a turbulent jet from the time-dependent constriction: if no energy is lost, exponential collapse to zero cross-sectional area is predicted, with no oscillations; if all the excess kinetic energy in the jet is lost, so that there is no pressure recovery downstream, steady flow is always possible and there are no oscillations; only if some energy loss and some pressure recovery are allowed are oscillations predicted.

The second group of theories is based on the experimental observation, e.g. by Brower & Scholten (1975), Griffiths (1977) and Bonis & Ribreau (1978), that breakdown of steady flow through the collapsible segment appears to occur only if the cross-sectionally averaged fluid velocity in the tube exceeds the local value of the speed of propagation of small-amplitude pressure waves, so that signals cannot be propagated upstream and the flow is 'supercritical'. The mechanism for the onset of unsteady behaviour is then analogous to the choking of sonic gas flow in a nozzle, and can be analysed by a one-dimensional model in which the elastic properties of the tube are represented by a 'tube law'; i.e. the transmural pressure at any point

is taken to be a single-valued function of the cross-sectional area at that point. The weakness of the lumped-parameter models is that they cannot incorporate wave propagation and therefore cannot distinguish between subcritical and supercritical flow. The weakness of most one-dimensional models is that, although they predict the onset of unsteady behaviour at a particular point in the tube, they have not been used to model the ensuing oscillations because they cannot incorporate either energy loss in the separated jet or the mechanical properties of the rigid tubes. An exception is the attempt by Reyn (1974), subsequently developed more fully by Shimizu & Tanida (1983), to analyse the motion in terms of the reflection of elastic jumps (analogous to shock waves) at the ends of the collapsible segment. Mention should also be made of the exhaustive study of unsteady flow in collapsible tubes, using one-dimensional theory, by Kamm & Shapiro (1979), who successfully modelled damped oscillations in a particular experiment but did not seek to model sustained, self-excited oscillations in a relatively short collapsible segment such as that of figure 1.

The purpose of the present paper is to show the development and the results of a new, composite model of a finite length of collapsible tube, incorporating both one-dimensional, wave-propagation effects and the important aspects of the lumped-parameter models. The model has two novel features which are important in the prediction of oscillatory behaviour. One is the inclusion of longitudinal wall tension in the description of tube elastic properties, and the other is a method of describing the energy loss in the separated jet in a way that is consistent with the one-dimensional flow equations. Despite these new features, the model remains qualitative, highlighting the main physical effects rather than attempting a precise simulation of every factor in an experiment. The model is developed in §2, the numerical method used to integrate the governing equations is outlined in §3, and the results are given in §4, for non-oscillatory cases, and §5, for cases in which self-sustained oscillations develop. Section 6 provides some preliminary comparisons with experiment.

2. The mathematical model

2.1. *The conventional one-dimensional equations*

In a one-dimensional theory the cross-sectional area A of the collapsible tube, the internal pressure p, and the cross-sectionally averaged longitudinal velocity $\bar{u}$ are taken to be functions of the longitudinal coordinate x and of time t. When a tube law exists, the elastic properties of the tube are represented by an equation of the form

$$p - p_e = \hat{P}(A), \tag{1}$$

where $p_e(t)$ is the chamber pressure, uniform but in general a function of time, and $\hat{P}(A)$ is a single-valued function which can in principle be determined by static measurements in the absence of flow; its shape in a particular experiment is shown in figure 2 (Kececioglu *et al.* 1981). Bertram & Pedley (1982) chose a form of $\hat{P}(A)$ that agrees with the well-known similarity solution for small A (Flaherty, Keller & Rubinow 1972), is very compliant for intermediate A, and is linear and stiff when the tube cross-section is circular. They took

$$\hat{P}(A) = K_p P(\alpha), \tag{2}$$

where $\alpha = A/A_0$, A_0 is the cross-sectional area when the tube cross-section is circular

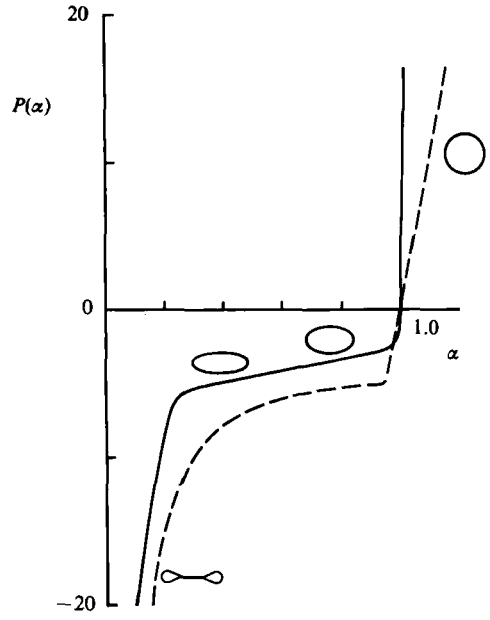

FIGURE 2. Dimensionless pressure–area relation for a uniform collapsible tube, showing cross-sectional shapes (after Kececioglu *et al.* 1981). Broken curve: equation (3*c*) with $k = 100$.

and unstretched, K_p is proportional to the circumferential bending stiffness, and $P(\alpha)$ is given by

$$P(\alpha) = 1-\alpha^{-\frac{3}{2}} \quad \text{for} \quad \alpha \leqslant 1, \tag{3a}$$

$$P(\alpha) = k(\alpha-1) \quad \text{for} \quad \alpha > 1, \tag{3b}$$

where k is a constant, taken here to be 100. In this paper we take a slightly modified form of this law, with continuous slope, as follows:

$$\begin{aligned} P(\alpha) &= k\{\alpha-a_2+a_3\,\mathrm{e}^{-a_1(\alpha-0.95)}\} \quad \text{for} \quad 0.95 < \alpha, \\ &= -(b_1+\alpha^{-1.5}) \qquad\qquad\quad \text{for} \quad \alpha > 0.95, \end{aligned} \tag{3c}$$

where

$$a_1 = 12.410926, \qquad a_2 = 1+a_3\,\mathrm{e}^{-0.05a_1},$$

$$a_3 = \left[\frac{1-1.5(0.95)^{-2.5}}{k}\right]\Big/a_1, \qquad b_1 = k(a_2-a_3-0.95)-(0.95)^{-1.5}.$$

This is 0 at $\alpha = 1$, agrees with (3*b*) for large α, and with (3*a*) for small α; it is plotted on figure 2.

The conservation-of-mass equation, for an incompressible fluid in a horizontal tube, is

$$A_t+(\bar{u}A)_x = 0, \tag{4}$$

where suffixes x, t denote partial differentiation. If the fluid is inviscid and the tube is slowly varying in x, so that the velocity profile is approximately flat and transverse velocities are negligible, the momentum equation is

$$\bar{u}_t+\bar{u}\bar{u}_x = -\frac{1}{\rho}p_x, \tag{5}$$

where ρ is the constant fluid density. From (1), the right-hand side of (5) can be rewritten as

$$-\frac{c^2}{A}A_x, \quad \text{where} \quad c^2 = \frac{A}{\rho}P'(A); \tag{6}$$

standard theory shows that c is the speed of propagation of small-amplitude waves in the absence of a mean flow.

At high values of the Reynolds number Re, viscous friction and energy dissipation have a relatively small effect when the flow is attached, unless the cross-sectional area becomes very small, and a large effect when flow separation has occurred. The standard one-dimensional models consider only attached flow, for which (5) is replaced by

$$\bar{u}_t + \bar{u}\bar{u}_x = -\frac{c^2}{A}A_x - F(A, \bar{u}, t)\,\bar{u}, \tag{7}$$

where the friction term F is positive. In our model the magnitude of the friction in regions of attached flow (i.e. upstream of the narrowest point in the tube) is not important. For the record, we used the following, quasi-steady estimates for F in such regions:

$$F = 8\pi\nu A^{-1} \quad \text{for } Re < 4000 \text{ and } A > A_0 \tag{8a}$$
(laminar flow, circular tube);

$$F = 8\pi\nu A_0 A^{-2} \quad \text{for } Re < 4000 \text{ and } A < A_0 \tag{8b}$$
(laminar flow, elliptical tube; see Wild, Pedley & Riley 1977);

$$F = 0.14\nu^{\frac{1}{4}}|\bar{u}|^{\frac{3}{4}}A^{-\frac{5}{8}} \quad \text{for } Re > 4000 \text{ and } A > A_0 \tag{8c}$$
(turbulent flow, circular tube; see Schlichting 1968 p. 561);

$$F = 0.14\nu^{\frac{1}{4}}|\bar{u}|^{\frac{3}{4}}\left(\frac{A^2}{A_0}\right)^{-\frac{5}{8}} \quad \text{for } Re > 4000 \text{ and } A < A_0 \tag{8d}$$
(turbulent flow, elliptical tube).

Note too that the inertia term in (7) should be modified whenever the velocity profile is not approximately flat (Rouse 1950, p. 57), and therefore retaining the term $\bar{u}\bar{u}_x$ is more valid for turbulent flow or for high-frequency unsteady flow than for quasi-steady laminar flow.

2.2. *Choking*

Here we consider steady flow, and suppose that at the upstream end ($x = 0$) of the collapsible segment the tube is distended ($A > A_0$) and $c > \bar{u} > 0$. The steady versions of (4) and (7), with (6), then yield

$$A_x = -\frac{F\bar{u}A}{c^2 - \bar{u}^2}. \tag{9}$$

Now $\bar{u}A$ is the constant flow rate, F is positive, and $c^2 > \bar{u}^2$ initially, so the right-hand side of (9) is negative. Thus A starts to decrease, and $\bar{u}$ will correspondingly increase. Moreover, the tube becomes more compliant as A decreases (figure 2), at least until A becomes very small, so c will decrease. Thus if the collapsible segment is long enough (and if $\bar{u}$ is not very much smaller than c, in which case the flow would probably be dominated by viscosity) a value of x will be reached at which $-A_x$ is predicted to be infinite. This leads to choking, and shows that steady flow is impossible if $\bar{u} = c$

anywhere; if that happens, the model must have broken down, and either unsteadiness develops or other neglected physical factors become important.

Even if choking does not develop because, for example, the collapsible segment is not long enough the model must still break down near the downstream end $x = L$, since A is less than the area of the downstream rigid tube and yet (9) still gives $A_x < 0$. Mathematically, (9) is a first-order equation for $A(x)$, and only one boundary condition (at $x = 0$ say) can therefore be satisfied once the flow rate $\bar{u}A$ has been specified. To increase the order of the equation we have to allow for longitudinal tension and curvature in the tube wall.

2.3. *Longitudinal tension*

A tube law of the form (1) cannot account for effects associated with longitudinal bending or stretching of the tube wall. Not only will non-uniform variations in cross-sectional area induce variable longitudinal stresses, but, whenever a tube is mounted as in figure 1, there is likely to be a considerable longitudinal tension in the walls even when there is no flow. If there is any longitudinal curvature, this will contribute to the transmural pressure. McClurken *et al.* (1981) discussed these various elastic effects, concluding that the initial longitudinal tension would in their experiments make the dominant contribution. We follow them and replace (1) by the following:

$$p - p_e = \hat{P}(A) - \frac{T}{R}, \tag{10}$$

where T is the longitudinal tension per unit perimeter, assumed to remain approximately constant (variations due to longitudinal viscous shear stress being neglected, for example), and R is a measure of the longitudinal radius of curvature, positive when most of the tube's cross-section is concave outwards (figure 1). Wall inertia, viscoelasticity, and many of the complicated details of large-deformation, non-axisymmetric shell theory are neglected in (10), which is still a very crude approximation. A precise specification of the relationship between R and the cross-sectional shape or area would therefore be inappropriate. We again follow McClurken *et al.* (1981) in recognizing that, where the tube is collapsed, the parts of the cross-section in which longitudinal tension will have most effect are approximately parallel-sided, at a distance y (say) from the plane of symmetry. We make one further simplification, taking y to be proportional to A, so that $1/R$ is finally given by

$$\frac{1}{R} = \frac{D_0 A_{xx}}{2A_0}\left[1 + \left(\frac{D_0 A_x}{2A_0}\right)^2\right]^{-\frac{3}{2}}, \tag{11}$$

where D_0 and A_0 are the diameter and cross-sectional area of the tube when it is circular and undeformed, and the factor $\frac{1}{2}$ arises because the wall is represented by two membranes.

2.4. *The separated-flow region*

In a lumped-parameter model, the energy loss associated with the separated jet can be represented by an equation for the pressure rise Δp between the narrowest point and the region of uniform velocity u_1 and area A_1 downstream, as a function of the area A_N at the narrowest point. Pedley (1980), for example, assumed that this energy loss was quasi-steady and used the well-known Borda–Carnot condition, deduced from momentum flux arguments, for the pressure rise downstream of an abrupt expansion:

$$\frac{\Delta p}{\rho} = +\left[\frac{A_1}{A_N} - 1\right] u_1^2. \tag{12}$$

The positive sign indicates some pressure recovery in the jet. However, such a lumped pressure change cannot be used in the present model, since our description of the elastic wall requires a knowledge of the continuous pressure distribution all the way to $x = L$, downstream of the narrowest point.

Instead, we note first that, in steady flow at least, the point of separation will be determined by the strength of the adverse pressure gradient in the expansion region. We therefore propose that, as collapse proceeds, separation will take place at the value of x, say x_s, at which $\partial p/\partial x$ first exceeds a critical value:

$$p_x > \frac{\gamma_1 \rho \bar{u}^2}{D_0}, \tag{13a}$$

where the dimensional scaling is based on the local dynamic pressure $\rho\bar{u}^2$ and the undisturbed tube diameter D_0 (the most easily available lengthscale), and γ_1 is a numerical constant. The value of γ_1 will depend on the local geometry: for Falkner–Skan flow with an adverse pressure gradient and with D_0 replaced by longitudinal distance x, $\gamma_1 \approx 0.09$ for incipient separation (Schlichting 1968, section IXa). Blasius's expansion for steady flow past a circular cylinder (diameter D_0) gives $\gamma_1 \approx 0.69$, while the Kármán–Pohlhausen method for flow past an elliptic cylinder with axis ratio 8:1 and major axis D_0 gives $\gamma_1 \approx 0.35$ (Schlichting, section IXc–d). In this paper we have arbitrarily taken $\gamma_1 = 0.3$; a check with $\gamma_1 = 0.2$ did not alter the qualitative behaviour (see below). It is assumed that the flow remains separated between $x = x_s$ and $x = L$, the downstream end of the collapsible segment, although this would not be true for a time of about $(L - x_s)/\bar{u}$. When the flow is slowing down or the collapse is becoming less severe, the flow will cease to be separated, the separation point being advected downstream. We account for this by requiring that the flow becomes attached again if, at $x = x_s$,

$$p_x < \frac{\gamma_2 \rho \bar{u}^2}{D_0}, \tag{13b}$$

where γ_2 is another constant (chosen equal to 0.05 or 0.1 here), smaller than γ_1 since there is hysteresis in the separation process. Thus the separation point can move downstream as well as upstream, according to the local pressure distribution. In some of our runs x_s was held fixed as soon as separation began for the first time (so the separated-flow region could not disappear), and this made a considerable difference.

In order to account for the energy loss in the diverging, separated-flow region, we again use momentum arguments, as follows. Write the x-component of velocity as $u = \bar{u} + u'$, where, by definition,

$$\int_A u' \, \mathrm{d}A = 0.$$

Integrating the x-component of the equation of motion across the tube (cf. (7)), we obtain

$$\bar{u}_t + \frac{\partial}{\partial x}\left(\tfrac{1}{2}\bar{u}^2 + \frac{p}{\rho}\right) + \frac{1}{A}\frac{\partial}{\partial x}\int_A u'^2 \, \mathrm{d}A = -F(A, \bar{u})\,\bar{u}, \tag{14}$$

as long as the normal component of velocity at the tube wall is negligibly small.

In steady flow, the diverging region immediately downstream of the separation point is characterized by a more or less parallel-sided jet (velocity u_0, say) surrounded

by an increasingly wide region of relatively stagnant fluid. The last term on the left-hand side of (14) is then approximately equal to

$$\frac{u_0^2 A_0^2}{A^3}\frac{\partial A}{\partial x} \approx -\frac{\partial}{\partial x}(\tfrac{1}{2}\bar{u}^2),$$

and is clearly positive. There is no pressure recovery in a parallel-sided jet; to allow for some pressure recovery, we take

$$\frac{1}{A}\frac{\partial}{\partial x}\int_A u'^2\,\mathrm{d}A = (\chi-1)\frac{\partial}{\partial x}(\tfrac{1}{2}\bar{u}^2) > 0, \tag{15}$$

where χ is a constant between 0 and 1, everywhere in the diverging region. If $\chi = 1$ there is no energy loss (no separation); if $\chi = 0$ there is no pressure recovery. The Borda–Carnot condition (12) is equivalent, on integration of (14), to choosing $\chi = 2/(1+A_1/A_N)$, which takes the value 0.18 when $A_N/A_1 = 0.1$, for example; in this paper we take $\chi = 0.2$ or 0.5. Note that this model is not valid in all flow configurations. For example, in a uniform tube, in which departures from fully developed flow decay with distance (such as the downstream rigid tube in our case), the quantity $\partial/\partial x \int_A u'^2\,\mathrm{d}A$ is negative and $\partial\bar{u}/\partial x$ is zero, so (15) cannot be used.

In unsteady flow there will be a time delay between the onset of separation and the development of the jet. Bertram & Pedley (1983) have measured this delay for the particular case of impulsively started flow in a two-dimensional indented channel, and found it to be approximately $7D_0/\bar{u}$. Here, however, we neglect such time delays and assume that the flow in the separated region (and hence the integral in (14)) is quasi-steady. Combining (14) and (15) we thus obtain

$$\bar{u}_t + \chi\bar{u}\bar{u}_x = -\frac{1}{\rho}p_x - F(A,\bar{u})\,\bar{u}. \tag{16}$$

This will be used in place of (7) in the separated-flow region (and, in general, F will be set to zero there because it has negligible effect for the parameter values chosen by us).

2.5. *Wave propagation*

The linearized version of the conventional model of §2.1, in the absence of friction but in the presence of a uniform mean flow with velocity $\bar{u}$, predicts that small-amplitude waves are propagated non-dispersively downstream with speed $c+\bar{u}$ and upstream with speed $c-\bar{u}$, where c is given by (6) evaluated at the undisturbed area $\bar{A}$. Hence no information can travel upstream if $\bar{u} \geqslant c$, which explains the choking phenomenon. It is instructive to calculate the possible speeds of wave propagation in a collapsible tube according to the present model, governed by equations (4), (10), (11) and (16), in place of (4), (1) and (5).

We perturb the variables A, $\bar{u}$, p by small quantities multiplied by $\mathrm{e}^{\mathrm{i}\kappa(c^*t-x)}$, substitute into the linearized equations and derive the following dispersion relation for the phase velocity c^*:

$$(c^*-\chi\bar{u})(c^*-\bar{u}) = c^2 + T'\kappa^2,$$

where c^2 is again given by (6) and $T' = TD_0\bar{A}/2\rho A_0$. The two solutions are

$$c^*_\pm = \tfrac{1}{2}[(1+\chi)\bar{u} \pm \{\bar{u}^2(1-\chi)^2 + 4c^2 + 4T'\kappa^2\}^{\frac{1}{2}}]; \tag{17a}$$

if there is no dissipation ($\chi = 1$) these reduce to

$$c^*_\pm = \bar{u} \pm (c^2 + T'\kappa^2)^{\frac{1}{2}}. \tag{17b}$$

The dependence on κ shows the waves to be dispersive. The group velocity is

$$c_{g\pm} = \frac{\mathrm{d}(\kappa c_{\pm}^*)}{\mathrm{d}\kappa} = c_{\pm}^* + \frac{2\kappa^2 T'}{\{(\bar{u}^2(1-\chi)^2 + 4c^2 + 4T'\kappa^2\}^{\frac{1}{2}}},$$

which has the same sign as $c_{\pm}^*$ except for a range of wavenumbers for which c_{-}^* is positive and c_{g-} negative. The main conclusion is that, however large $\bar{u}$ is compared with c, there is a value of κ sufficiently large that c_{-}^* and c_{g-} are negative. In other words, the presence of longitudinal tension allows perturbations to travel upstream in the form of short-wavelength waves. A fuller discussion of wave propagation in collapsible tubes with longitudinal tension is given by McClurken *et al.* (1981).

We should also note that, even when the longitudinal tension is negligible ($T' = 0$), it is possible, according to this model, for waves to propagate upstream in the region of separated flow where $\chi < 1$ even when $\bar{u} > c$. From equation (17*a*) it can be shown that $c_{-}^* < 0$ if $\bar{u} < c/\sqrt{\chi}$; thus for $\chi = 0.2$, upstream-propagating waves are possible for values of $\bar{u}/c$ up to about 2.2.

2.6. *Boundary and initial conditions*

The system of governing equations – (4), (10), (11) and (16) – is fourth order in x, so four boundary conditions are required. Two of these come from the requirement that the cross-sectional area of the collapsible tube must equal that of the rigid tubes at each end (A_1). The other two introduce the mechanical properties of the rigid parts of the system, because the given flow parameters are the pressure P_{R} in a static reservoir far upstream, and atmospheric pressure (zero) far downstream. The pressure drop across each rigid tube will consist of a resistive term, taken proportional to the square of the flow rate because of the presence of constrictive control valves (Conrad 1969, and figure 1), and an inertial term, taken as an effective length times the fluid acceleration. The four boundary conditions are thus:

$$A(0,t) = A_1; \tag{18a}$$

$$A(L,t) = A_1; \tag{18b}$$

$$p(0,t) = p_{\mathrm{R}} - \tfrac{1}{2}\rho\bar{u}^2(0,t) - \rho L_1 \bar{u}_t(0,t) - k_1 A_1^2 \bar{u}^2(0,t); \tag{18c}$$

$$p(L,t) = k_2 A_1^2 \bar{u}^2(L,t) + \rho L_2 \bar{u}_t(L,t). \tag{18d}$$

In all the numerical calculations to be described, we take the initial state to be one in which the collapsible segment has uniform area A_1, and in which friction is negligible within the collapsible segment so that the velocity is uniform and subcritical, with a given value $\bar{u}_1$ less than the value of c given by (6) when $A = A_1$:

$$A(x,0) = A_1, \quad \bar{u}(x,0) = \bar{u}_1. \tag{19}$$

The corresponding value of p_{R}, held fixed in the subsequent computations, is then given by (18*c*, *d*) to be

$$p_{\mathrm{R}} = \{\tfrac{1}{2}\rho + (k_1 + k_2) A_1^2\} \bar{u}_1^2; \tag{20}$$

the initial value of p_{e} is given by (10) and (18*d*) to be

$$p_{\mathrm{e}0} = k_2 A_1^2 \bar{u}_1^2 - P(A_1). \tag{21}$$

Collapse of the tube is then initiated by increasing p_{e} over a short time t_0 to a higher constant value:

$$p_{\mathrm{e}} - p_{\mathrm{e}0} = p_{\mathrm{e}1} \frac{t}{t_0} \quad \text{for} \quad 0 \leqslant t \leqslant t_0,$$

$$= p_{\mathrm{e}1} \quad \text{for} \quad t \geqslant t_0. \tag{22}$$

Also the friction function F (8) is switched on at $t = 0$, if required. Numerical integration is performed for $t > 0$. In some cases a steady state is eventually set up and in some cases oscillations develop.

2.7. *Non-dimensionalization*

The scales used for non-dimensionalization are as follows: lengths D_0; area A_0; velocity $c_0 = (kK_p/\rho)^{\frac{1}{2}}$; pressure, ρc_0^2; time D_0/c_0. Note that c_0 is the speed of wave propagation given by (6) when $A = A_0$ and $P(\alpha)$ is given by (3*b*). The dimensionless wave speed in general is given by $c^2 = \alpha P'(\alpha)/k$. We introduce $\alpha = A/A_0$ (cf. (3)), write $u = \bar{u}/c_0$ and retain p, t and x for dimensionless pressure, time and longitudinal coordinate. The governing equations and boundary conditions become

$$\alpha_t + (u\alpha)_x = 0; \tag{23}$$

$$u_t + (\chi)\, uu_x = -p_x - fu, \tag{24}$$

where χ (§2.4) is different from 1 only in the separated-flow region, and $f(\alpha, u, t) = D_0 F/c_0$, with F given by (8) in the attached-flow region;

$$p - p_e = \frac{1}{k} P(\alpha) - \frac{\sigma}{2} \alpha_{xx} (1 + \tfrac{1}{4}\alpha_x^2)^{-\frac{3}{2}}, \tag{25}$$

where $\sigma = T/\rho c_0^2 D_0$ and $P(\alpha)$ is given by (3*c*);

$$\alpha(0, t) = \alpha(\lambda, t) = \alpha_1, \tag{26a, b}$$

where $\alpha_1 = A_1/A_0 \geqslant 1$, $\lambda = L/D_0$;

$$p(0, t) = p_R - \tfrac{1}{2}u^2(0, t) - \eta_1 \alpha_1^2 u^2(0, t) - \lambda_1 u_t(0, t), \tag{26c}$$

$$p(\lambda, t) = \eta_2 \alpha_1^2 u^2(\lambda, t) + \lambda_2 u_t(\lambda, t), \tag{26d}$$

where $$\eta_{1,2} = \frac{k_{1,2} A_0^2}{\rho}, \quad \lambda_{1,2} = \frac{L_{1,2}}{D_0}, \quad p_R = [\tfrac{1}{2} + (\eta_1 + \eta_2)\alpha_1^2]\, u_1^2;$$

and $$\alpha(x, 0) = \alpha_1 \geqslant 1, \quad u(x, 0) = u_1 < c_1 = \alpha_1^{\frac{1}{2}}. \tag{27}$$

The initiation of the motion is given by (22).

2.8. *Parameter values*

It is not intended to give exhaustive coverage of all possible parameter values, but merely to demonstrate qualitative behaviour in a particular example that is typical of experiments such as Conrad's (1969).

The lengths of the two rigid tubes are taken to be the same, at various values ($\lambda_1 = \lambda_2 = 1, 2, 10$ or 20), while the collapsible tube segment is taken to be 5 or 20 diameters long ($\lambda = 5$ or 20). The associated resistance constants are chosen to be: $\eta_1 = 50$ or ∞ (the latter representing a constant inflow rate at $x = 0$), $\eta_2 = 40$ or 50. The area of the rigid tubes is taken to be the same as, or 10% greater than, the undeformed area of the collapsible tube: $\alpha_1 = 1.0$ or 1.1 (this variation has negligible effect). The inflow velocity is taken to be very subcritical: $u_1 = 0.05$ or 0.1. The constant k, representing the stiffness of the elastic tube when distended (3*b*), takes the value of 100 (Bertram & Pedley 1982) and the longitudinal tension parameter σ is given the value 1, 2, 4 or 0.2. The dimensionless pressure p_{e1} by which p_e is raised to start the collapse (22) is usually taken to be 0.05, although one run was done with

$p_{e1} = 0.2$; note from (21) that p_{e0} takes the value 0.051 when $\alpha_1 = 1.1$, $u_1 = 0.05$, $\eta_2 = 50$. The dimensionless time t_0 over which p_e is raised is taken to be 10.

In envisaging the experiments, we assume dimensional values of $A_0 = 1$ cm^2 ($D_0 = 1.13$ cm), $c_0 = 100$ cm s^{-1}, $\rho = 1$ g cm^{-3}, $\nu = 0.011$ cm^2 s^{-1}. These values are inserted into the friction function F (8) when the flow is unseparated. We recall that, in the separated-flow region, χ (24) is given the value 0.2 or 0.5, while the critical pressure gradients for the initiation or disappearance of separation are represented by the constants (13*a*, *b*) $\gamma_1 = 0.3$ or 0.2, $\gamma_2 = 0.05$ or 0.1.

3. Numerical method

3.1. *Finite-difference scheme*

The pressure is eliminated from the governing equations by substituting (25) into (24), so that, if the region $0 \leqslant x \leqslant \lambda$ is divided into n segments of length $\Delta x = \lambda/n$, there are $2n$ variables whose time variation must be described. These are $u_j = u(j\,\Delta x, t)$ for $j = 1, 2, \ldots, n+1$, and $\alpha_j = \alpha(j\,\Delta x, t)$ for $j = 2, 3, \ldots, n$; $\alpha_{(1)}$ and $\alpha_{(n+1)}$ are given by (26*a*, *b*). The $2n$ equations from which these unknowns are calculated consist of $2n-2$ finite-difference representations of (23) and (24, 25) at the internal points ($j = 2, 3, \ldots, n$), and the two equations representing the pressures at the ends: (26*c*, *d*), with (25) to eliminate p again. Most of our computed results were obtained with $\Delta x = 0.5$; accuracy was verified by varying it between 0.125 and 1.0.

To integrate the equations we have used an adaptation of the MacCormack finite-difference scheme (Roache 1972, p. 253), which is an explicit two-level predictor–corrector scheme, often used for solving hyperbolic equations. It is second-order accurate in both Δx and Δt, the time step. The choice of Δt is made from considerations of numerical stability. We always took

$$\Delta t \leqslant \frac{\left(\frac{c^2}{\alpha}\right)_{\max} \frac{1}{(c+|u|)_{\max}}}{\left(\frac{c^2}{\alpha}\right)_{\max} \frac{1}{\Delta x} + \frac{1}{2}\frac{\sigma}{(\Delta x)^3}}, \tag{28}$$

where $c = [\alpha P'(\alpha)/k]^{\frac{1}{2}}$ is the dimensionless wave speed; (28) reduces to the standard stability criterion in the purely hyperbolic case when $\sigma = 0$ and, while not rigorously proved, was shown empirically to ensure stability when $\sigma \neq 0$.

The procedure for cases in which the flow separates is to calculate at each time step the finite-difference representation of p_x/u^2 (13*a*, *b*), using a centred difference for p_x. As t increases, this quantity will first exceed γ_1 at a particular t and at some values of x, the smallest of which we call x_s; for all x in the range $x_s \leqslant x \leqslant \lambda$ the parameter χ (24) is immediately reduced from 1 to the chosen separated-flow value. In some runs x_s was held fixed thereafter. However, at later times, p_x/u^2 may exceed γ_1 at smaller values of x, so in the full model x_s is allowed to fall. Later still, p_x/u^2 may fall below γ_2 at x_s and for a range of larger x ($x_s \leqslant x \leqslant x_s'$ say) and in that case *either* χ is restored instantaneously to the value 1 for all x in that range *or* x_s is convected downstream with the local flow velocity: considering x_s as a function of t we have

$$x_s(t+\Delta t) = x_s(t) + u(x_s, t)\,\Delta t, \tag{29}$$

where in fact the closest grid-point to (29) is chosen.

3.2. *Reliability of steady and unsteady solutions*

Whenever the time-dependent solution tends eventually to a steady state, that steady state is completely reliable. Even with the large Δx value of 0.5, the equilibrium flow rate and (in cases where dissipation was suppressed) total head are uniform to within 2% (1% if α remains above 0.15), an error which is reduced by reducing Δx.

The reliability of the transient phase of the solution is less certain, as there is no overall check like that of uniform flow rate. However, as long as the numerical stability criterion (28) is satisfied and Δx is sufficiently small, we find that the solution is independent of Δx and Δt, at least for components of the disturbance that have wavelengths significantly greater than Δx. An example is shown in figure 3, where u is plotted as a function of time, at two different values of x, for a case in which a steady state eventually develops. The different symbols represent two values of Δx ($= 0.5$ and 0.25), with corresponding Δt values differing by a factor of about 4, and it can be seen that the two sets of points lie on the same curves.

These results are not conclusive, however, when it comes to the prediction of oscillations. We find (§5) that oscillations normally develop as a result of the coupling between pressure waves and the position of the separation point in the flow just downstream of the narrowest point. In almost all the cases we considered, holding this point fixed leads to the development of a steady state which is therefore stable. The question arises whether, in ensuring that our finite-difference scheme is *numerically* stable, we have not suppressed *physical* instabilities, such as those predicted by lumped-parameter models. To investigate the answer, we have (*a*) performed a linearized stability analysis of the predicted steady flow, solving the resulting ordinary differential equations numerically (§3.3), and (*b*) analysed the lumped-parameter system that most closely represents our model, to see when that predicts instability (see Appendix), and then integrated our equations for the same parameter values.

The lumped-parameter model predicts (oscillatory) instability only if the downstream resistance η_2 is extremely small (less than 0.344 for the parameter values chosen), and the flow does not then need to be supercritical. A numerical solution of the full model for the same parameter values is shown in figure 4, and indeed reveals the existence of oscillations for a subcritical flow and a fixed separation point. The amplitude of the oscillations is very small, the cross-sectional area at the narrowest point remaining close to 0.38, and the dimensionless period is approximately 5.2. In order to ensure accuracy for these computations, Δt was reduced to 0.1 times the value given by (28). The predictions of the lumped model are that the equilibrium area is 0.372, in good agreement with figure 4, and that the period of oscillation is about 41.4, in poor agreement.

We conclude that the full numerical model predicts oscillations when the parameter values are such as to yield oscillations from the lumped-parameter model, which suggests that it does not necessarily suppress physical instabilities other than the one discussed in §5. This view is reinforced by the results of the stability analysis of the next section.

3.3. *Stability of the steady state*

In order to investigate the stability of one of the computed steady states we write the dependent variables as a mean, x-dependent, value plus a small perturbation, e.g.

$$u(x,t) = U(x) + u'(x,t).$$

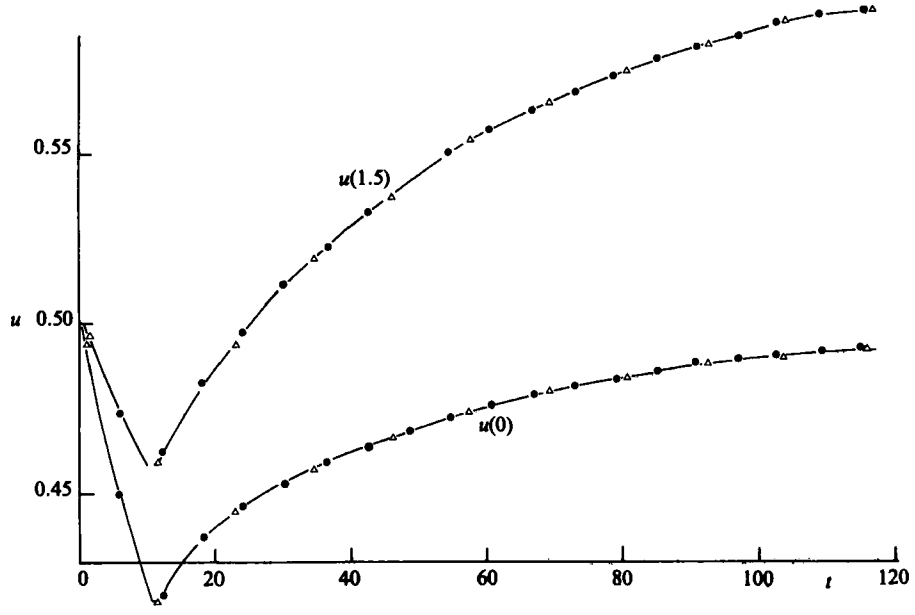

FIGURE 3. Plots of $u(0,t)$ and $u(1.5,t)$ for a case in which a steady state develops, showing the agreement between calculations using $\Delta x = 0.5$ (●—●) and 0.25 (△—△). Parameter values: $\alpha_1 = 1$, $\lambda_1 = \lambda_2 = 2$, $\lambda = 5$, $\eta_1 = \eta_2 = 50$, $\sigma = 1$, $u_1 = p_{e1} = 0.05$, $f = 0$, $\chi \equiv 1$.

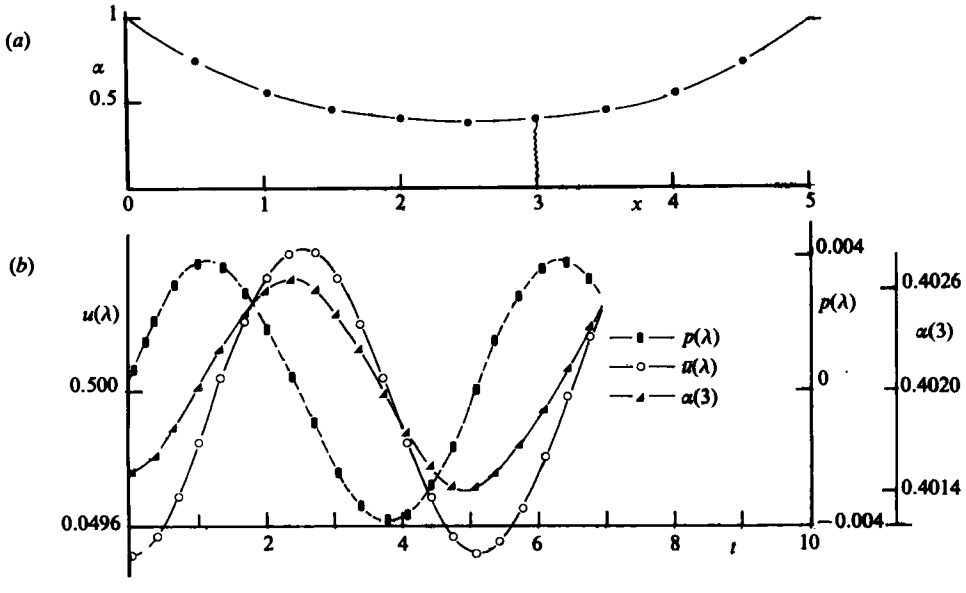

FIGURE 4. A case of subcritical oscillations, as predicted by the lumped-parameter model. (*a*) $\alpha(x,t)$: the oscillations are invisible on this scale; the mark at $x = 3$ represents the separation point. (*b*) $p(\lambda,t)$, $u(\lambda,t)$, $\alpha(3,t)$. Parameter values: $\alpha_1 = 1$, $\lambda_2 = \lambda = 5$, $\lambda_1 = \eta_1 = \infty$, $\eta_2 = 0$, $\sigma = 0.2$, $u_1 = p_{e1} = 0.05$, $f = 0$.

Substitution into the governing equations and boundary conditions (23–26), linearization, and discretization of the x-variable into n steps leads to the following system of $2n$ ordinary differential equations:

$$\frac{\mathrm{d}\omega_i}{\mathrm{d}t} = V_{ij}\omega_j, \tag{30}$$

where ω_i is the $2n$-vector $(u_1', u_2', \ldots, u_{n+1}', \alpha_2', \ldots, \alpha_n')$ and V_{ij} is a $2n \times 2n$ matrix whose components depend on the steady solution and the parameters of the system. If any of the eigenvalues of V_{ij} has positive real part, then the steady state is predicted to be unstable. These eigenvalues were determined numerically, the functions $U(x)$ etc. also being computed from the steady-state solution of the original initial-value problem. Note that, in this stability calculation, the separation point x_s was held fixed at its steady-state value.

In computing the components of V_{ij}, it is necessary to evaluate the x-derivatives of u' and α'. It immediately becomes apparent that how these derivatives are numerically evaluated is crucial to the results. For example, if upwind differences are taken, the perturbations are independent of the properties of the downstream rigid tube (η_2, λ_2), and, if downwind differences are taken, they are independent of the upstream-tube properties (η_1, λ_1). Either must be wrong, because the acceleration in, say, the downstream rigid tube must depend on the inertance of that tube, etc. Some form of mixed differencing must therefore be used.

We used three different schemes to calculate the elements of V_{ij}:

(i) central differences in both continuity and momentum equations;

(ii) upwind differences in the momentum equation and downwind differences in the continuity equation;

(iii) upwind differences in the momentum equation and central differences in the continuity equation.

If the computed eigenvalues of V_{ij} are approximately the same for each scheme, we can be confident of the results. In fact, however, only about a third of the $2n$ eigenvalues, those corresponding to the lowest frequency or longest wavelength disturbances, are satisfactorily reproduced when the differencing scheme is changed. Many of the rest are completely different. Of the reproducible eigenvalues, none has a positive real part, but some of the irreproducible ones do have positive real parts. However, as n is increased, the reproducible eigenvalues are repeated while the irreproducible ones are not. The eigenvalues with positive real part shift towards higher frequencies. We conclude, therefore, although without absolute certainty, that the instabilities associated with the irreproducible eigenvalues have no physical meaning and that the computed steady states are stable. Hence we can have confidence in the numerical scheme for solving the full equations and presume it does not suppress any genuine physical oscillations.

4. Results and discussion: non-oscillatory cases

4.1. *No dissipation in the collapsible segment*

We first examine the collapse process when there is assumed to be neither viscous friction ($f \equiv 0$) nor flow separation ($\chi = 1$). Results are presented in figures 5–8 for the case in which $\lambda_1 = \lambda_2 = 1$, $\eta_1 = \eta_2 = 50$, $\sigma = 2$, $k = 100$, $\alpha_1 = 1$, $\lambda = 20$, $p_{e1} = 0.05$, $u_1 = 0.1$. The time t_0 over which the external pressure is raised from p_{e0}

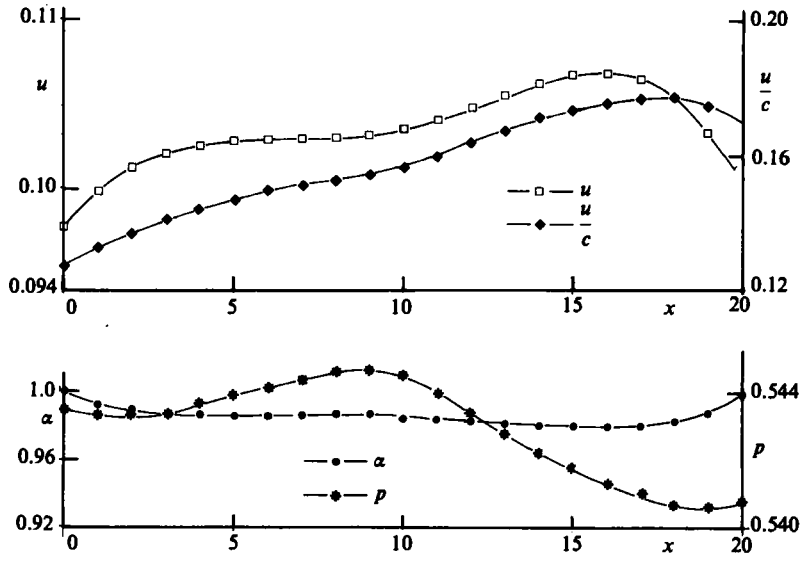

FIGURE 5. Development of collapse when there is no dissipation in the collapsible tube; u, u/c, p, α are plotted against x for $t = 35.8$. Parameter values: $\alpha_1 = 1$, $\lambda_1 = \lambda_2 = 1$, $\lambda = 20$, $\eta_1 = \eta_2 = 50$, $\sigma = 2$, $u_1 = 0.1$, $p_{e1} = 0.05$, $f = 0$, $\chi \equiv 1$.

to $p_{e0}+p_{e1}$ (22) is equal to 10 units, about half the time for a long wave to travel the length of the collapsible segment, at least while $c \approx 1$, before collapse. The inlet value of u/c is at first equal to 0.146.

The uniform increase in external pressure is initially accompanied by a uniform increase in internal pressure, and no flow. However the boundary conditions (26c, d) cause waves of lower pressure to propagate in from the ends, with a corresponding reduction in area: the velocity is reduced at $x = 0$ and increased at $x = \lambda$. After these waves have met in the middle, α falls almost uniformly (except near the ends). This is shown in figure 5, where α, p, u and u/c are plotted against x at $t = 35.8$. The pressure in the centre of the tube, initially uniform and equal to 0.5, is falling from its maximum value of 0.55 because of the waves. The slight asymmetry of the p- and α-distributions is a consequence of fluid inertia, since u_t is negative at the upstream end and positive at the downstream end. Note that $u(0, t)$ has fallen below u_1 by about 5%, and $u(\lambda, t)$ has risen by about 4%. The flow is very subcritical, because u/c is everywhere less than 0.18.

As long as the flow remains subcritical, the collapse proceeds in a nearly symmetrical manner, as can be seen from figure 6, where the same quantities as in figure 5 are plotted at $t = 1254$. There is still slight asymmetry in p and α, and from the u-curve we can see that the inflow velocity is still slightly below its initial value, and the outflow velocity slightly above. In cases where we chose either a significantly smaller inlet velocity ($u_1 = 0.05$) or a significantly larger longitudinal tension ($\sigma = 4$) a steady state was eventually set up, looking much like figure 6 except that it was completely symmetrical because of the lack of dissipation in the collapsible segment. It is the presence of dissipation in the rigid segments that makes a steady state possible.

In the case shown, however, this did not happen because the flow became critical. Figure 6 shows u/c very close to 1 in the middle of the tube (in fact the value at which new behaviour begins is a little larger than 1 because of the influence of the

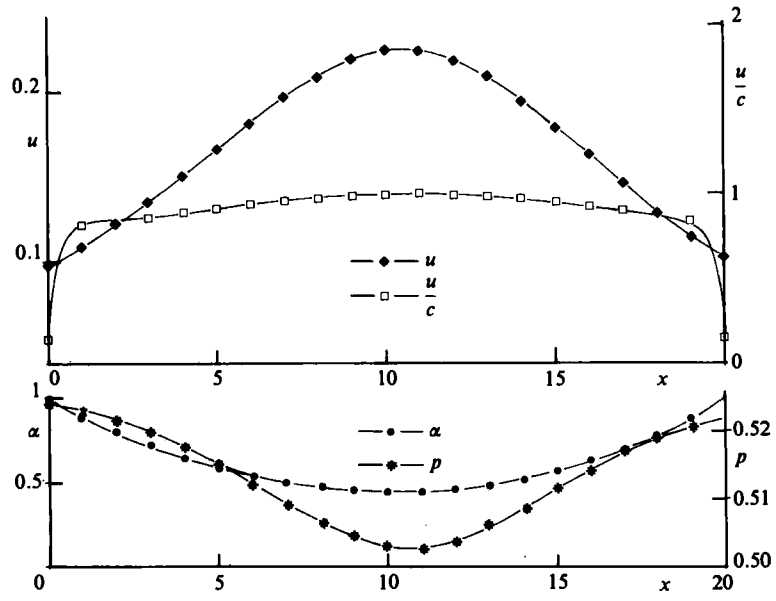

FIGURE 6. As figure 5, at $t = 1253.85$.

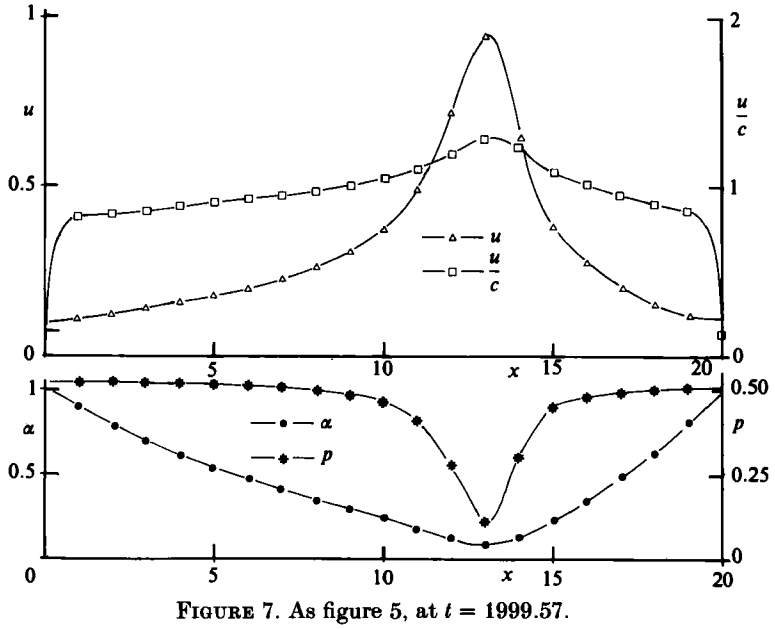

FIGURE 7. As figure 5, at $t = 1999.57$.

longitudinal tension). A little later, a critical value was exceeded, and the collapse process changed completely. Figure 7 shows the position at $t = 2000$. The fall in area near the narrowest point is associated with a marked favourable pressure gradient upstream of it. However, this is inadequate to accelerate the fluid to the velocity that would be required by a uniform steady flow rate, so α at the narrowest point must continue to fall, by conservation of mass. Downstream of the narrowest point there is an adverse pressure gradient associated with the area expansion, but this is not enough to slow down the velocity; the fluid is further accelerated, and the downstream

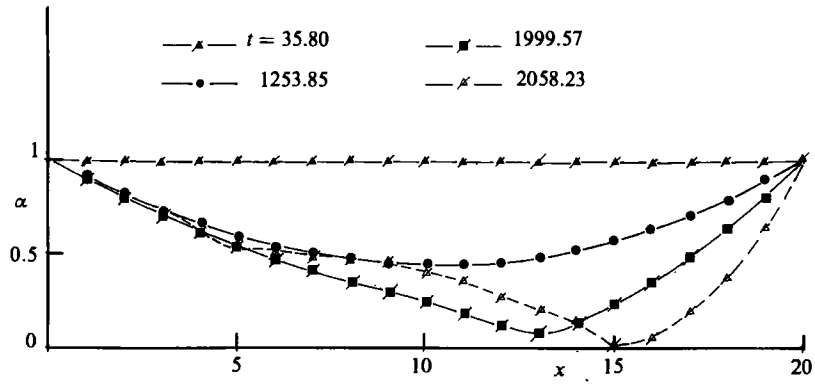

FIGURE 8. α plotted against x for four values of t. Parameter values as in figure 5.

section of the tube is emptied increasingly rapidly. Combined with a slight reflation upstream, this means that the narrowest point moves downstream while the area at it decreases. The presence of longitudinal tension allows short waves to propagate upstream, causing fluctuations in velocity and pressure at the inlet, but these do not alter the collapse process overall.

In the absence of dissipation in the collapsible segment, this process, once started, inevitably continues until the area at the narrowest point reaches zero; in the present example this occurs just after $t = 2058$. Figure 8 shows plots of α as a function of x at this time as well as those plotted already. The nearly complete collapse, and the reflation upstream, are obvious.

That complete collapse is inevitable follows from the requirement in steady flow (flow rate q, say) that $H = p + \frac{1}{2}q^2/\alpha^2$ be uniform. In the state represented by figure 7, H is greater at the narrowest point than just upstream, so, for H to become uniform, p must decrease more rapidly, as α decreases, than $q^2/2\alpha^2$ increases. In other words, $\mathrm{d}p/\mathrm{d}\alpha$ must be greater than $q^2/\alpha^3 = u^2/\alpha$. But $\mathrm{d}p/\mathrm{d}\alpha \approx c^2/\alpha$, since the longitudinal tension term cannot become very large at small α, from (25) and the definition of c. Hence the collapse cannot be halted while $c < u$.

4.2. *Influence of dissipation: flow limitation*

The presence of dissipation in the collapsible tube permits the outflow velocity to be slowed down relative to the inflow velocity so that a steady state is possible, although it may be unstable and lead to oscillations – see §5. We first consider what happens when all the new dissipation is associated with flow separation, so that $f \equiv 0$ and $\chi < 1$ in (24) for $x > x_s$. Oscillations were avoided by holding x_s fixed during the transient collapsing phase and adjusting it gradually to the correct position (given by (13*a*) with $\gamma_1 = 0.3$) once the steady state was reached. No qualitative difference is observed in cases where the dissipation-free calculation leads to a steady state. However the complete collapse predicted above for cases of supercritical flow is halted. The steady-state distributions of α, u and $H = p + \frac{1}{2}u^2$ (total head) are plotted in figure 9 for $\chi = 0.2$ (curves *a*) and 0.5 (curves *b*), other parameters being as in figures 5–8.

The most striking feature of these results is that the steady-state flow rate is virtually unaffected by the value of χ or η_2: although the $u(x)$ distribution is greatly affected, the eventual steady value of $u(0)$ or $u(\lambda)$ is almost identical with the more or less constant value of $u(0, t)$ seen in figures 5–7. This is consistent with the fact that, when the flow becomes supercritical, long waves cannot propagate upstream from

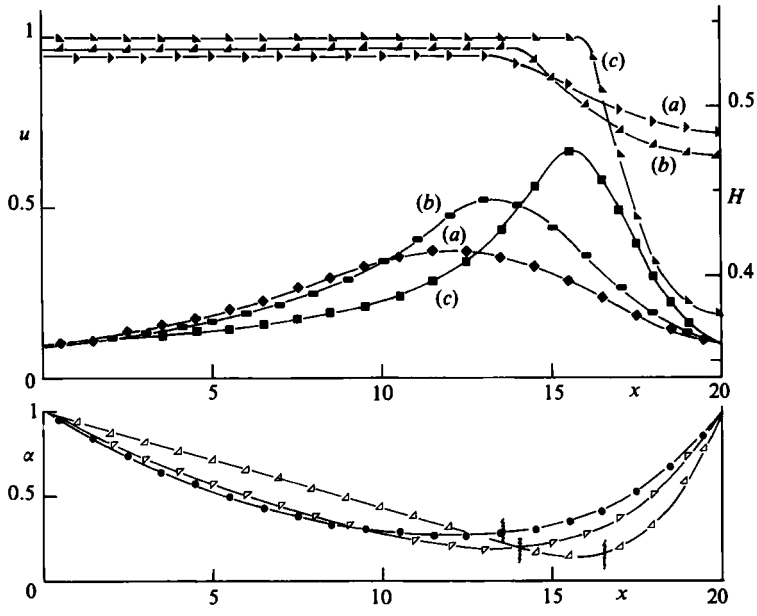

FIGURE 9. Steady-state solutions when there is dissipation due to flow separation: plots of $H = p + \frac{1}{2}u^2$ (closed triangles), u (closed rectangles), α against x. Marks on the α-curves indicate the points of flow separation. Parameter values: $\alpha_1 = 1$, $\lambda = 20$, $\eta_1 = 50$, $\sigma = 2$, $u_1 = 0.1$, $p_{e1} = 0.5$, $f = 0$, $\gamma_1 = 0.3$. Curves (*a*) $\eta_2 = 50$, $\chi = 0.2$; (*b*) $\eta_2 = 50$, $\chi = 0.5$; (*c*) $\eta_2 = 40$, $\chi = 0.2$.

the narrowest region, so that the adjustment of the flow takes the form of a downstream deceleration. Thus, if the flow becomes supercritical, the steady-state flow rate remains the same whatever happens downstream: this is 'flow limitation' (Dawson & Elliott 1977). In fact, although it cannot be seen in figure 9, the flow rate is slightly lower for the higher value of χ, which seems surprising, since larger χ means less dissipation per unit length, other things being equal. However, we see from figure 9 that, when χ is larger, the collapse proceeds further before it is arrested (the narrowest area becomes smaller and moves downstream) and the *total* dissipation is somewhat larger (see the total head curves).

Further evidence of flow limitation is seen from curves (*c*) of figure 9, for which the parameters are the same as for curves (*a*) except that the downstream resistance of η_2 has been reduced from 50 to 40. This reduction of downstream resistance means that the pressure near $x = \lambda$ falls, so that the collapse point moves downstream and the narrowest area becomes smaller. A corresponding reflation takes place upstream of the collapsed region, and the flow rate again remains almost constant, falling very slightly.

Steady-state solutions can also be obtained with direct viscous friction as well as (or instead of) flow separation. However, curves (*a*) of figure 9 are not noticeably affected by the inclusion of the friction term, and we conclude that it is unimportant for realistic parameter values.

The usual sort of evidence of flow limitation consists of graphs of the pressure drop across the collapsible segment, $p(0) - p(\lambda)$, against the steady-state flow rate $u\alpha$, when the pressure difference $p(0) - p_e$ is held constant (Lambert & Wilson 1972). In figure 10 we show an almost equivalent plot, in which p_e is held constant but instead of $p(0)$ it is the driving pressure $p_R = [\frac{1}{2} + (\eta_1 + \eta_2)\alpha_1^2]u_1^2$ that is held constant. The

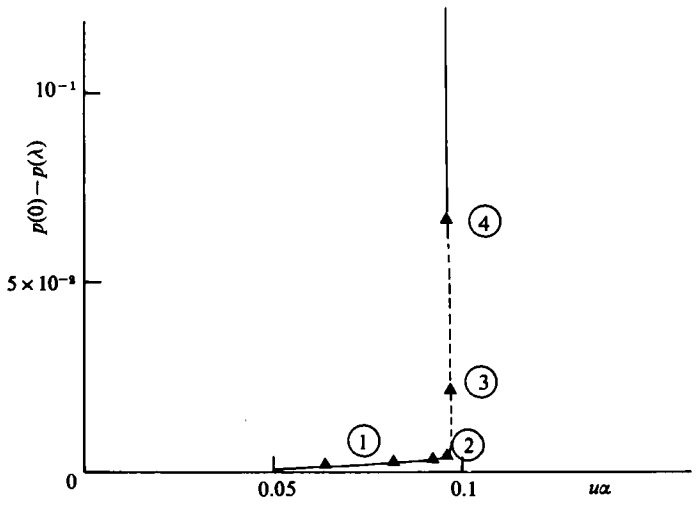

FIGURE 10. Flow limitation: plot of $p(0)-p(\lambda)$ against $u\alpha$ when the flow is steady. For explanation of regions 1, 2, 3, 4 see text. Parameter values: $\alpha_1 = 1$, $\lambda = 20$, $\lambda_1 = \lambda_2 = 10$, $\eta_1 = 50$, $\sigma = 2$, $\chi = 0.2$, $\gamma_1 = 0.3$, $p_e = 0.554$, $p_R = 1.009$, $f \neq 0$; η_2 was varied from 200 to 30.

downstream pressure $p(\lambda)$ is varied by allowing η_2 to decrease from 200 to 30. In the region of the curve with $u\alpha < 0.5$, the tube is slightly inflated. In region 1 there is a slight indentation but no flow separation, and the slight rise of $p(0)-p(\lambda)$ with $u\alpha$ is a consequence of laminar friction (which is included in this case). At point 2 the flow first separates and there is a discontinuous jump to point 3. Continuous passage from 3 to 4 ($\eta_2 = 50$) is also not possible because choking occurs there. From 4 onwards, the tube is dramatically collapsed along almost all its length, and further reduction in η_2 is in fact accompanied by a slight *decrease* of flow rate (a phenomenon well known to respiratory physiologists in the context of forced expiration, and referred to as 'negative effort dependence').

5. Results and discussion: sustained oscillations

5.1. *The prediction of oscillations*

We have seen that small-amplitude oscillations may arise when the flow is subcritical if the resistance of the downstream rigid segment is sufficiently small (figure 4), as predicted by lumped-parameter models (Appendix). However, most experimentalists report oscillatory behaviour if and only if the flow becomes supercritical somewhere. When the lumped model predicts stability, our model predicts stable, steady, supercritical flow if the point of flow separation x_s is prevented from moving during the collapse process (§4.2). We now present the results of the full model in which x_s is allowed to move according to the local value of the adverse pressure gradient, as specified in §2.4. We found oscillations in every case examined for which the flow became supercritical anywhere (we also found some oscillations in some subcritical flows for which *stability* was predicted by the lumped model, but these were again of very small amplitude: see below). Moreover the generation of these oscillations is found to be intrinsic to the collapsible tube and cannot be accounted for by the lumped-parameter model. Quantitative aspects of the oscillations, such as amplitude and frequency, may be influenced by the rest of the flow circuit, but their existence is not.

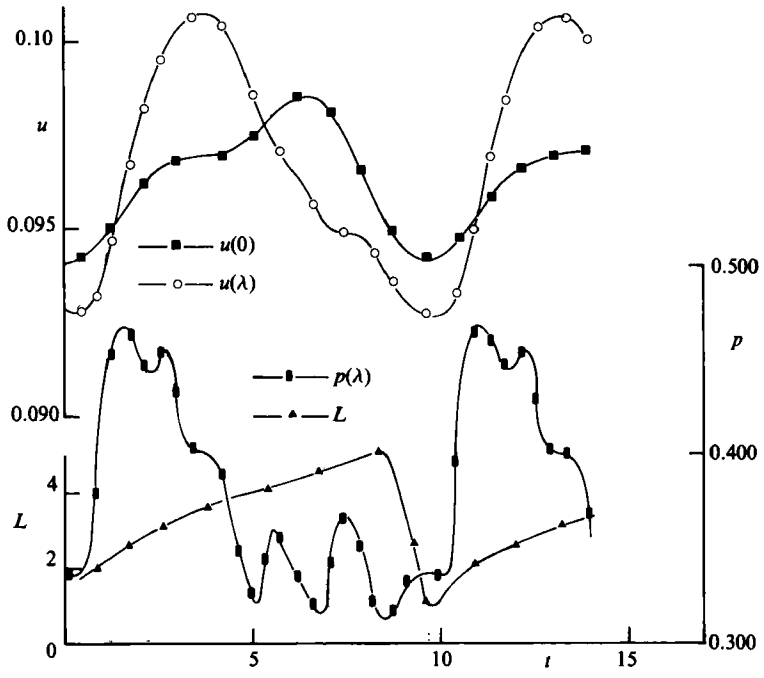

FIGURE 11. Self-excited oscillations for the case in which the (unstable) steady state is shown in curves (*c*) of figure 9: plots of $u(0,t)$, $u(\lambda,t)$, $p(\lambda,t)$ and $L = \lambda - x_s$ against t. Additional parameter: $\gamma_2 = 0.05$. Separation disappears suddenly (see text).

We begin by reconsidering the case for which the steady state is depicted in curves (*c*) of figure 9; the additional parameter values are $\eta_1 = 50$, $\lambda_1 = \lambda_2 = 20$, and γ_2, which defines the pressure gradient at which separation ceases (13*b*), $= 0.05$. The results are plotted in figures 11 and 12: figure 11 shows $u(0,t)$, $u(\lambda,t)$, $p(\lambda,t)$ and $L = \lambda - x_s$ (the distance of the separation point from the downstream end of the collapsible segment) as functions of t; figure 12 shows α and p as functions of x at different times t. To save computing time the initial condition for these calculations was taken to be the steady state with $\eta_2 = 50$ (curves (*a*) of figure 9); η_2 being reduced to 40 at $t = 0$. Oscillations have clearly developed. Their amplitude is not large (the peak-to-trough value for $u(\lambda,t)$ being about 0.008), but is considerably larger than in the subcritical case of figure 4. The period of the oscillations is about 9.5 units, and the maximum value of $\lambda - x_s$ is about 5: the period is thus comparable with the time that a wave of speed 1 would take to propagate from the furthest upstream separation point to the outlet ($x = \lambda$) and back again.

Figures 11 and 12 show that the velocity and pressure amplitudes at $x = 0$ are less than those at $x = \lambda$, which is consistent with the fact that long waves cannot be propagated upstream when the flow is supercritical. Because of longitudinal tension, however, short waves can overcome this restriction, and we observe them particularly in the graphs of p against x. It is the oscillation in $\lambda - x_s$ which above all exemplifies the nature of the oscillations; if after a certain time it is held fixed, the oscillations in the other quantities die away.

In the calculations of these figures, the disappearance of separation when p_x at x_s falls below its critical value (13*b*) was sudden: χ was immediately set equal to 1 for the whole range $x_s \leqslant x < x_s'$ for which p_x is below its critical value. In later

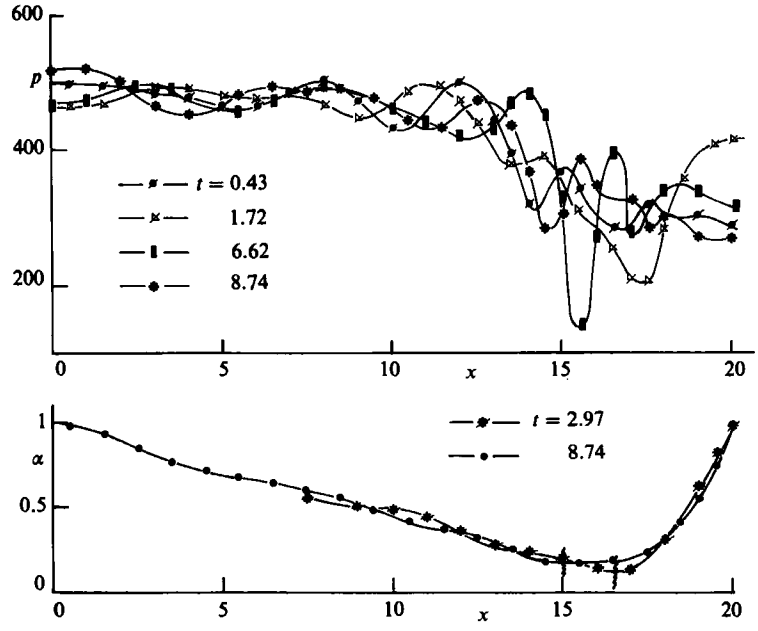

FIGURE 12. Plots of p and α against x for various values of t, for the case shown in figure 11.

calculations the separation point was convected downstream at the local fluid velocity, as given by (30). In that case graphs corresponding to figures 11 and 12 are shown in figures 13 and 14. Oscillations still occur, albeit with slightly smaller amplitude (0.006 in $u(\lambda, t)$) and larger period (about 12 units); the main difference is the smoother variation of $\lambda - x_s$.

Varying the other parameters associated with separation (χ, γ_1, and γ_2) also affects the quantitative details of the oscillations to a slight extent, but, as long as x_s is allowed to vary and the flow becomes supercritical somewhere, qualitatively similar oscillations always occur. It is not the purpose of this paper to provide a thorough study of the effects of varying all the parameters of the model, and we restrict ourselves to three observations.

(i) The value of 2.0 chosen as the standard for the longitudinal tension parameter σ is somewhat larger than one would expect to find in an experiment (see §6 below). In one run with the smaller value of $\sigma = 0.2$ there were considerable numerical difficulties, mainly because the constriction is moved much closer to the downstream end of the collapsible segment and there is a very rapid expansion downstream, with a short separated-flow region. The computation could be successfully performed only with a larger value of η_2 than that used in figures 11–14: 50 rather than 40. However, the oscillations in $u(\lambda, t)$ are not greatly affected: the amplitude is reduced to about 0.004 and the period increased to about 16. The oscillations in $u(0, t)$ are considerably reduced, as expected since a lower tension means less upstream wave propagation.

(ii) Increasing the excess external pressure p_{e1} has the obvious effect of reducing the minimum mean area. Oscillations still occur unless p_{e1} is so large that the divergent portion of the tube near $x = \lambda$ is too short for variations of x_s to be possible (in our model, x_s has to vary by at least Δx before oscillations can occur). In figure 15 results are shown for the case $p_{e1} = 0.2$, and we see that the amplitude of the oscillations has fallen, the period has increased, and the oscillations have become more irregular, when compared with figure 11.

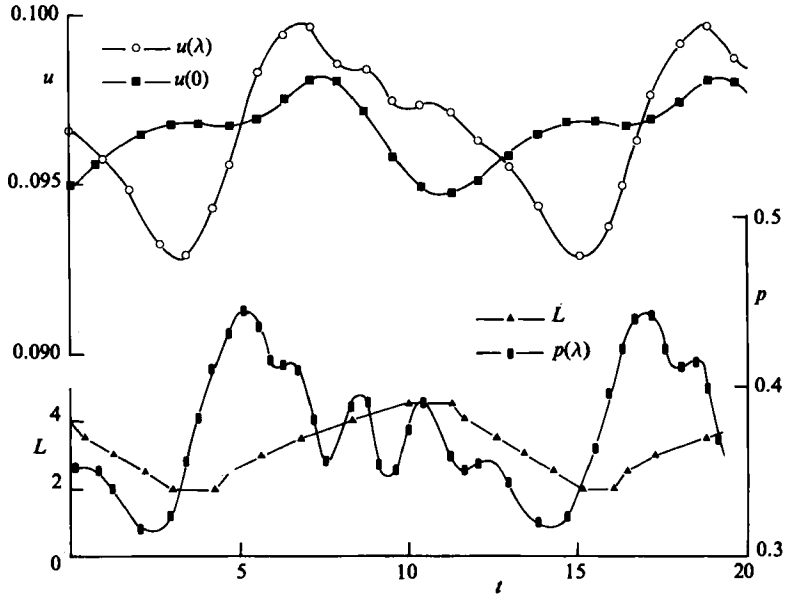

FIGURE 13. As figure 11, except that separation disappears gradually.

(iii) The quantitative details of the oscillations when they occur clearly depend on the conditions in the upstream and downstream rigid segments (see Conrad *et al.* 1978 and Pedley 1980), although their excitation by the present mechanisms is unaffected. In figure 16 we show the oscillations in $u(0,t)$, $u(\lambda,t)$, $p(0,t)$ and $p(\lambda,t)$ for the case in which $\lambda_1 = \lambda_2 = 1$, other quantities being the same as in figure 11. The amplitude of the velocity oscillations has increased, to 0.016 for $u(\lambda,t)$, and they are more nearly in phase with the pressure oscillations, as one would predict for small inertia, but the general shape is the same as in figure 11, and so is the period (9.5).

Finally we demonstrate that oscillations can be predicted even when the flow is subcritical everywhere and the lumped model indicates stability, as long as the separation point is allowed to vary. However, they have extremely small amplitude, and no clear demarcation between states with and without oscillations has been identified. An example is shown in figures 17 and 18 for a case in which the parameters are the same as in figure 11 except that $\eta_2 = 50$ and $u_1 = 0.05$ instead of 0.1.

We see that the amplitude in $u(\lambda,t)$ is down to 0.0007 but that the oscillations have become rather irregular and of much longer period. The fact that the flow is subcritical is reflected in the longer wavelengths of the waves upstream of the narrowest point (figure 18). It should be noted that these oscillations are not robust and may be quite unphysical, because in order to find them at all we had to reduce γ_1 to 0.2 (from 0.3) and raise γ_2 to 0.1 (from 0.05). Moreover, the predicted amplitudes of these oscillations and those of figure 4 are so small as to make them virtually undetectable.

5.2. *Detailed dynamics of the oscillations*

The dynamics of the oscillations can be discussed with reference to the pressure curves in figure 14. At $t = 3.00$ the pressure gradient in the outlet region is largely favourable, and we expect the separation point to have been moving downstream. The plot of L against t in figure 13 confirms that x_s reaches its furthest downstream position a little after this time.

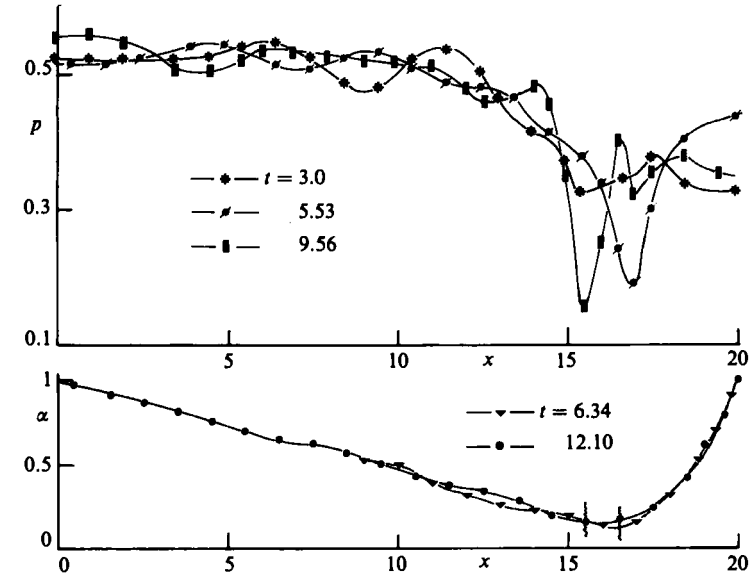

FIGURE 14. As figure 12, except that separation disappears gradually.

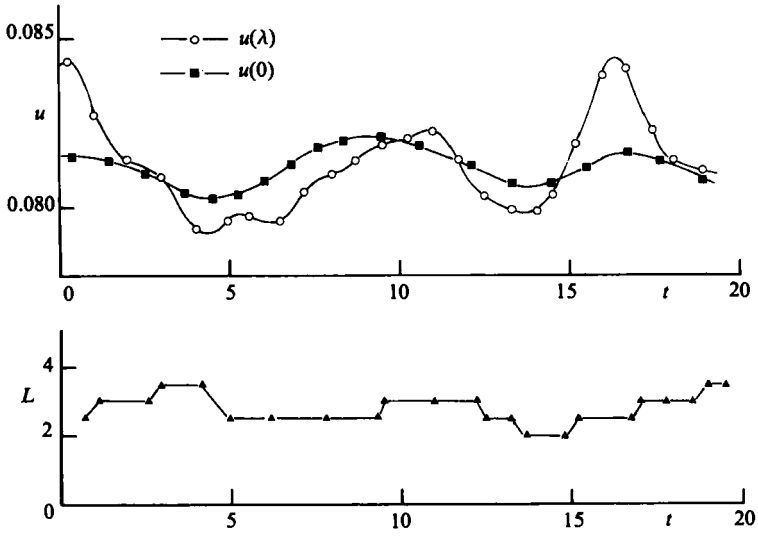

FIGURE 15. Oscillations with a larger external pressure. Plots of $u(0,t)$, $u(\lambda,t)$, $L(t)$. Parameter values as in figure 11, except $p_{e1} = 0.2$.

As the separation point moves downstream, the flow emerging from the constriction remains attached for a greater distance and the local flow rate (and hence u) increases: in other words $u_t > 0$ there. This accelerating, reattached flow acts like a piston and sends a high-pressure wave downstream and a low-pressure wave upstream towards the constriction. (We have avoided the phrases 'compression wave' and 'expansion wave' because, for example, the low pressure in an expansion wave is associated with small cross-sectional area and it would look as if the tube were being compressed.) The fluid immediately downstream of the constriction is sucked downstream, so that the constriction itself narrows and moves towards the outlet.

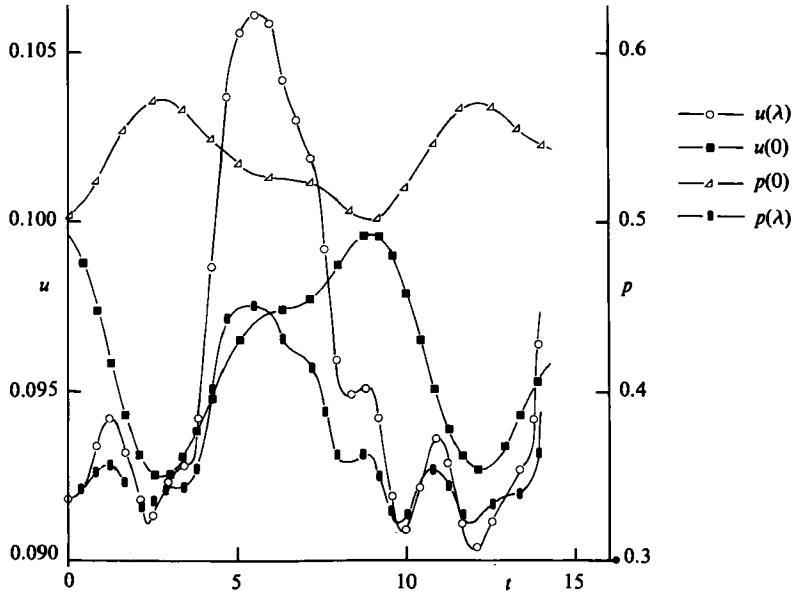

FIGURE 16. Oscillations with less inertia in the rigid parts of the system. Plots of $u(0,t)$, $u(\lambda,t)$, $p(0,t)$, $p(\lambda,t)$. Parameter values as in figure 11, except $\lambda_1 = \lambda_2 = 1$.

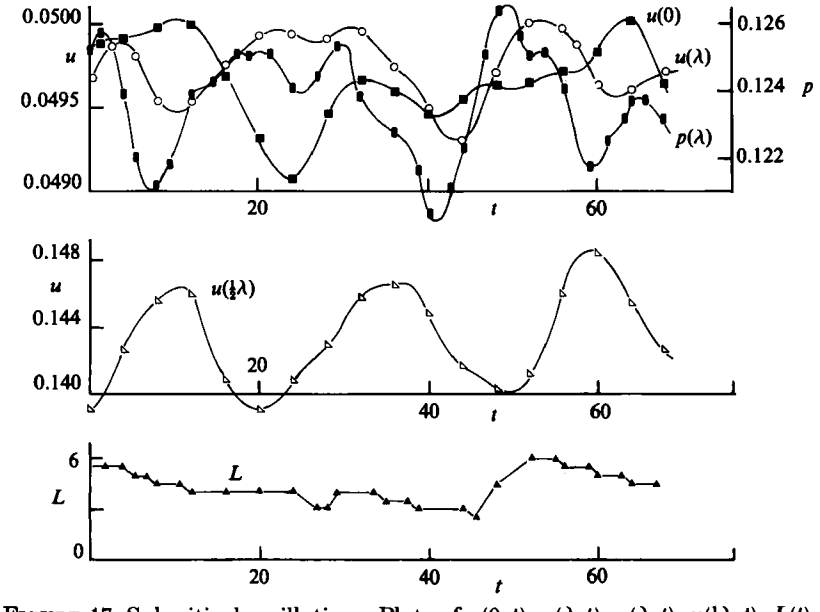

FIGURE 17. Subcritical oscillations. Plots of $u(0,t)$, $u(\lambda,t)$, $p(\lambda,t)$, $u(\frac{1}{2}\lambda,t)$, $L(t)$. Parameter values as in figure 11 except $\eta_2 = 50$, $u_1 = 0.05$.

When the high-pressure wave reaches the outlet ($x = \lambda$) there is a build-up of pressure there as the wave is reflected, and an adverse pressure gradient is established (see the pressure curve at $t = 5.53$ in figure 14). This first halts and then reverses the motion of the separation point. As the separated-flow region spreads backwards the average velocity starts to fall again. This time a high-pressure wave moves upstream

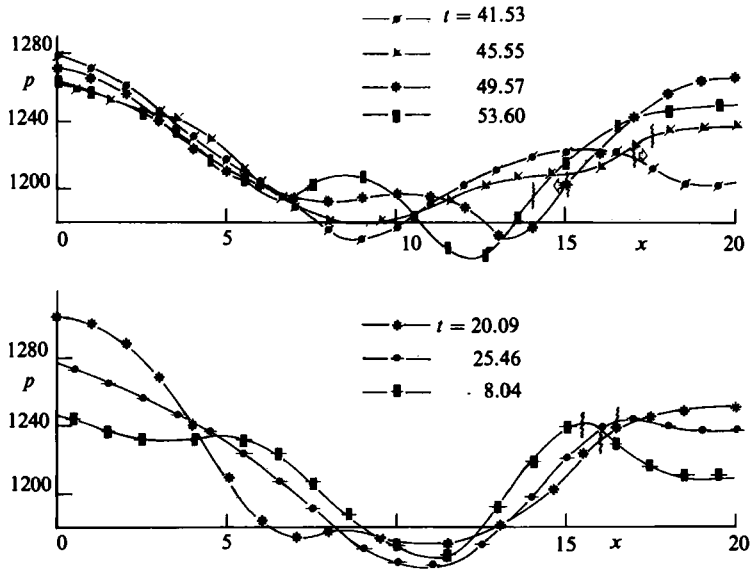

FIGURE 18. Plots of p against x for various times t, during the oscillations depicted in figure 17.

to be superimposed on the reflected wave, and a low-pressure wave moves downstream. However, if the flow upstream of the separation point is supercritical, the upstream-moving waves cannot proceed far. They tend to pile up, generating a pressure maximum which pushes the separation point further upstream. (The piling-up effect will be somewhat mitigated by the presence of longitudinal tension, which enables short waves to propagate upstream to the inlet: however, these have relatively small amplitude, as can be seen from figure 14.) The pressure maximum will be associated with an increase in area, so during this phase the constriction will become less severe and will move upstream (see pressure curves at $t = 9.56$ and area curve at $t = 12.1$, when the separated-flow region is longest).

This phase too must come to an end. The downstream-moving low-pressure wave reduces the pressure at the outlet, diminishing the outflow velocity $u(\lambda, t)$, which by $t = 9.56$ has already passed its maximum value (figure 13). A train of low-pressure waves is generated at the outlet, and moves upstream. These waves overtake the high-pressure waves where they are piled up, and cause the pressure maximum to fall, weakening the adverse pressure gradient. This can be seen clearly by comparing the $t = 6.62$ and the $t = 8.74$ pressure curves of figure 12. At the later time the pressure rise has moved upstream but its magnitude has been sharply reduced. The separation point is now at its furthest upstream; a little later, the pressure gradient becomes too weak for separation to occur and the separation point moves downstream again. Then the whole cycle restarts.

In summary, the key mechanism of the oscillations is the movement of the separation point in response to the local pressure gradient. It moves upstream when a high-pressure wave is moving up from the outlet, and moves downstream again when the strength of that wave is diminished by the low-pressure wave that follows. The reason that the oscillations are much stronger when the flow is supercritical is also clear: the pressure peak cannot propagate far upstream and is therefore readily caught by the following trough. In supercritical flow the period of the oscillations is clearly related to the time of travel of a wave from the constriction to the outlet and back.

6. Concluding remarks

Ideally, we would now compare our predictions with experiment, showing to what extent the frequency and waveform of the predicted oscillations agrees with those observed. Unfortunately, not only does our model still contain numerous simplifications, but none of the authors who describe self-excited oscillations give enough of the experimental parameters for a good simulation. In particular, very few papers quote any elastic parameters, even the Young's modulus E of the tube wall, although linear elasticity theory gives the following estimates for the dimensional parameters:

$$K_p = \frac{E(2h/D_0)^3}{12(1-n^2)}, \quad k = \frac{3}{2}\left(\frac{D_0}{h}\right)^2, \quad \rho c_0^2 = kK_p = \frac{Eh}{(1-n^2)D_0}, \; T = \epsilon Eh, \tag{31}$$

where h is the wall thickness, n is the Poisson's ratio and ϵ is the longitudinal strain. Lyon *et al.* (1981) are the only authors to quote values for ϵ ($0 < \epsilon < 0.67$) but do not give E. Note that the given estimate for T gives $\sigma = (1-n^2)\epsilon$, $= 0.75\epsilon$ when $n = \frac{1}{2}$ as for an incompressible material.

The non-dimensionalization of this paper scales the period of the oscillations, $1/\Omega$, with the time for a wave to travel a distance of one diameter, when the tube is distended and the speed is c_0. The oscillations, however, occur when the tube is collapsed and the wave speed, $\tilde{c}$ say, is much smaller. Moreover the relationship between $\tilde{c}$ and c_0 depends very much on the form of $P(\alpha)$, which is likely to vary markedly from one experiment to another; the forms (3*a–c*) chosen by us are highly idealized. In making comparison with experiment, therefore, we consider the value of the quantity $\mathscr{P} = \tilde{c}/\Omega D_0$, where $\tilde{c}$ is the wave speed evaluated at $\alpha = \tilde{\alpha}$, a small value. In our model, $\tilde{c}^2 = 1.5(K_p/\rho)\tilde{\alpha}^{\frac{3}{2}}$, and we shall choose $\tilde{\alpha} = 0.1$, close to the minimum predicted value (figure 12), so that

$$\frac{\tilde{c}}{c_0} \approx \left(\frac{47.4}{k}\right)^{\frac{1}{2}}. \tag{32}$$

Thus the predicted dimensionless periods of 9–16 are equivalent (with $k = 100$) to $\mathscr{P} = 6.2$–11.0. It should be borne in mind that, in comparing predicted and experimental values of $\mathscr{P}$, we are assuming that its dependence on other dimensionless quantities (the precise value of $\tilde{\alpha}$, σ, $\tilde{u}/\tilde{c}$, λ, etc.) is slight, which may not be true.

Authors who quote frequencies and give some information on elastic parameters include Conrad (1969), Bonis (1979) and Bertram (1982). From Conrad's data and (31) we compute $k = 2.8 \times 10^4$, $c_0 = 1.25$ m s^{-1} and $D_0 = 1.27$ cm. He quotes oscillation frequencies 0.5–1.0 Hz, which are equivalent to values of $\mathscr{P}$ in the range 4–8, quite close to our predicted range. The data of Bonis (1979) lead to $k = 1500$ and $c_0 = 7.22$ m s^{-1} ($D_0 = 1.14$ cm). He describes two sorts of supercritical oscillation, a 'high-frequency' vibration localized near the outlet and a large-amplitude oscillation of much lower frequency, with a period ranging between 1.5 and 15 s. The latter are equivalent to $\mathscr{P}$ values between 169 and 1690, which are far above our predictions. Bertram (1982), with $k = 19$, $c_0 = 21$ m s^{-1} (assuming that E has the same value as for Bonis), and $D_0 = 1.25$ cm, also reports two types of oscillation: high-frequency vibrations ($\Omega = 30$–40 Hz) and low-frequency 'milking' oscillations, in which the constriction first appears in the upstream half of the tube and then propagates, becoming more pronounced, toward the downstream end. The frequency of these oscillations is 2–3 Hz. The corresponding values of $\mathscr{P}$ are 884–1327 for the milking oscillations and 66–88 for the high-frequency vibrations. These results suggest that it is the vibrations that, if anything, are simulated in our model.

Ur & Gordon (1970) quote very few parameters, but give excellent detailed records of $p(0,t)$ and $p(\lambda,t)$ during the oscillations. The shape of the $p(\lambda,t)$ waveform is qualitatively similar to that shown in figure 11, in that there is a double peak occupying about $\frac{1}{3}$ of the cycle, followed by a relatively quiescent phase. They quote oscillation frequencies Ω of 12–50 Hz which, if we *assume* parameters similar to those of Bonis (1979), are equivalent to dimensionless periods $\mathscr{P} = 2.3$–9.4.

The above comparisons emphasize the difficulty in trying to use the present qualitative model to simulate particular experiments. The feature of the model that most clearly requires improvement is the modelling of the head loss in the separated-flow region, because it ignores the inevitable lag time between the initiation of separation and the full development of energy dissipation in the jet. In the experiments of Bertram & Pedley (1983) this lag time has a dimensionless value of around 7, comparable with the predicted period of oscillation. The next generation of models should incorporate such a lag, although one hopes that a more complete description of the dissipation process can also be developed. However, we believe that the oscillation mechanism highlighted in this paper is both new and relevant to collapsible-tube experiments.

Dr Cancelli is most grateful to the Accademia Nazionale dei Lincei, who supported him during his visit to Cambridge in 1981, when most of the work described in this paper was performed.

Appendix. A lumped-parameter model

We combine the principal features of the models of Schoendorfer & Shapiro (1977) and of Pedley (1980). The collapsible tube is represented two-dimensionally as a pair of circular membranes (figure 19), separated by a dimensionless distance $\alpha(t)$ at the narrowest point (the same non-dimensionalization is used as in §2.7). The elastic properties are modelled by superimposing a tube law relating $p(t)$ (internal pressure at the narrowest point) $-p_e$ to α and a term representing longitudinal tension (cf. (25)):

$$p-p_e = \frac{P(\alpha)}{k} - \frac{4\sigma(\alpha_1-\alpha)}{(\alpha_1-\alpha)^2+\lambda^2} \approx \frac{P(\alpha)}{k} - \frac{4\sigma(\alpha_1-\alpha)}{\lambda^2}. \tag{A 1}$$

For convenience, we restrict attention to the case in which the inflow to the collapsible segment u_1 is held fixed; this is equivalent to taking infinite upstream resistance η_1. The velocities at the narrowest point and in the downstream rigid tube are taken to be $u(t)$ and $u_2(t)$ respectively. The fluid-mechanical equations, simplified by the assumption $\lambda \gg \alpha_1$ in calculating the volume contained in the collapsible segment, are as follows:

Conservation of mass:

$$\alpha_1(u_1-u_2) = \tfrac{1}{3}\lambda\dot{\alpha}, \tag{A 2}$$

$$\alpha_1 u_1 - \alpha u = \tfrac{1}{6}\lambda\dot{\alpha}. \tag{A 3}$$

Momentum equations:

$$p-p_2 = u_2^2 - \frac{\alpha u^2}{\alpha_1}, \tag{A 4}$$

$$p_2 = \eta_2 \alpha_1^2 u_2^2 + \lambda_2 \dot{u}_2, \tag{A 5}$$

where, in (A 4), only the separated-flow dissipation is included, as suggested by the results of §4, and the Borda–Carnot condition has been used in place of χ = constant (if χ is taken constant, the lumped-parameter model is always unstable).

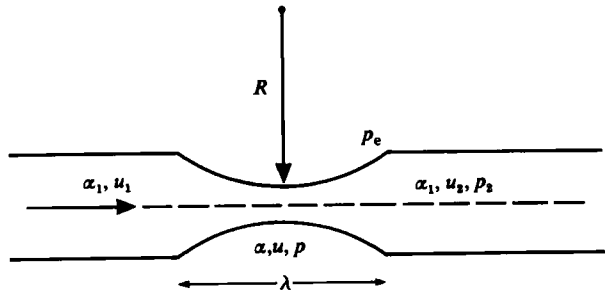

FIGURE 19. Sketch of the lumped-parameter model, indicating dimensionless areas, velocities, pressures, and two lengths. The radius of curvature $R = [\lambda^2+(\alpha_1-\alpha)^2]/4(\alpha_1-\alpha)$.

This system admits of a steady state in which $u_2 = u_1$, $u = \alpha_1 u_1/\bar{\alpha}$, and $\alpha = \bar{\alpha}$, where

$$p_e+\frac{P(\bar{\alpha})}{k}-\frac{4\sigma}{\lambda^2}(\alpha_1-\bar{\alpha}) = \left[\eta_2\alpha_1^2+1-\frac{\alpha_1}{\bar{\alpha}}\right]u_1^2. \tag{A 6}$$

We investigate the stability of this equilibrium by setting $\alpha = \bar{\alpha}+\alpha' e^{\beta t}$ in (A 1)–(A 5), where $\alpha' \ll \bar{\alpha}$, and linearizing to give the following quadratic equation for β:

$$c_2\beta^2+c_1\beta+c_0 = 0, \tag{A 7}$$

where

$$\begin{aligned} c_2 &= \frac{\lambda\lambda_2}{3\alpha_1} > 0, \\ c_1 &= \frac{\lambda u_1}{3}\left(2\eta_2\alpha_1+\frac{2}{\alpha_1}-\frac{1}{\bar{\alpha}}\right), \\ c_0 &= -\frac{u_1^2\alpha_1}{\bar{\alpha}^2}+\frac{4\sigma}{\lambda^2}+\frac{P'(\bar{\alpha})}{k}, \end{aligned} \tag{A 8}$$

and, from (2b), $P'(\bar{\alpha}) = \frac{3}{2}\bar{\alpha}^{\frac{5}{2}}$. Graphical analysis of (A 6) shows that, when $\bar{\alpha}$ is the smallest root with $\bar{\alpha} < 1$, then $\mathrm{d}/\mathrm{d}\bar{\alpha}$ of the left-hand side is greater than that of the right-hand side, and hence $c_0 > 0$. Thus a root of (A 7) can have positive real part, implying instability, only if $c_1 < 0$; the root is complex, implying oscillatory instability, if in addition $c_1^2 < 4c_0c_2$.

As in the main text, we write $p_e = p_{e0}+p_{e1}$, where p_{e0} is the value required to make $\alpha = \alpha_1$ an equilibrium state. Then the equilibrium area whose stability we investigate is, from (A 6), given by

$$p_{e1}+\frac{P(\bar{\alpha})-P(\alpha_1)}{k}-\frac{4\sigma}{\lambda^2}(\alpha_1-\bar{\alpha}) = \left(1-\frac{\alpha_1}{\bar{\alpha}}\right)u_1^2. \tag{A 9}$$

For numerical purposes we use parameter values typical of the examples considered in the main text: $\lambda = \lambda_2 = 5$, $\alpha_1 = 1$, $k = 100$, $u_1 = p_{e1} = 0.05$, $\sigma = 0.2$ and η_2 we do not specify as yet. These numbers give $\bar{\alpha} = 0.372$. We see immediately from (A 8) that $c_1 < 0$ only if $\eta_2 < 0.344$, and in that case $c_1^2 < 4c_0c_2$. In other words, the equilibrium is stable unless the downstream rigid tube has very small resistance; in that case there is an oscillatory instability and self-excited oscillations would be expected to ensue. An estimate of the (dimensionless) period of the oscillations is

$$\frac{2\pi}{|\operatorname{Im}\beta|} = 4\pi c_2(4c_0c_2-c_1^2)^{-\frac{1}{2}},$$

which takes the value 41.4 for the above parameters. These conclusions would still be true in the absence of longitudinal tension ($\sigma = 0$), when the model reduces essentially to the constant-inflow model of Pedley (1980) or Bertram & Pedley (1982). We see that it is the resistance of the downstream rigid tube that governs the stability, and for values as high as those used in plotting figures 5–16, for example, no instability is predicted. When instability is predicted, it is independent of whether the flow in the collapsible tube becomes critical or not; in fact, for the numbers used here, the maximum value of u/c, equal to $[ku_1^2/\alpha^3 P'(\alpha)]^{\frac{1}{2}}$, is 0.52.

REFERENCES

Bertram, C. D. 1982 Two modes of instability in a thick-walled collapsible tube conveying a flow. *J. Biomech.* **15**, 223–224.

Bertram, C. D. & Pedley, T. J. 1982 A mathematical model of unsteady collapsible tube behaviour. *J. Biomech.* **15**, 39–50.

Bertram, C. D. & Pedley, T. J. 1983 Steady and unsteady separation in an approximately two-dimensional indented channel. *J. Fluid Mech.* **130**, 315–345.

Bonis, M. 1979 Écoulement visqueux permanent dans un tube collabable elliptique. Thèse de Doctorat d'État, Université de Technologie de Compiègne.

Bonis, M. & Ribreau, C. 1978 Étude de quelques propriétés de l'écoulement dans une conduite collabable. *La Houille Blanche* **3**, **4**, 165–173.

Brower, R. W. & Scholten, C. 1975 Experimental evidence on the mechanism for the instability of flow in collapsible vessels. *Med. Biol. Engng* **13**, 839–845.

Cancelli, C. & Chiocchia, G. 1979 On the onset of self-excited oscillations in a collapsible tube flow with sonic index values less than one: mathematical model and numerical results. *Atti d. Acc. Naz. dei Lincei, Memorie Sc. Fisiche, sez. I*, **15**, 317–352.

Conrad, W. A. 1969 Pressure–flow relationships in collapsible tubes. *IEEE Trans. Bio-med. Engng BME-16*, 284–295.

Conrad, W. A., Cohen, M. L. & McQueen, D. M. 1978 Note on the oscillations of collapsible tubes. *Med. Biol. Engng & Comput.* **16**, 211–214.

Conrad, W. A., McQueen, D. M. & Yellin, E. L. 1980 Steady pressure flow relations in compressed arteries: possible origin of Korotkoff sounds. *Med. Biol Engng & Comput.* **18**, 419–426.

Dawson, S. V. & Elliott, E. A. 1977 Wave-speed limitation on expiratory flow – a unifying concept. *J. Appl. Physiol.: Respirat. Environ. Exercise Physiol.* **43**, 498–515.

Flaherty, J. E., Keller, J. B. & Rubinow, S. I. 1972 Post-buckling behaviour of elastic tubes and rings with opposite sides in contact. *SIAM J. Appl. Maths* **23**, 446–455.

Griffiths, D. J. 1977 Oscillations in the outflow from a collapsible tube. *Med. Biol. Engng & Comput.* **15**, 357–362.

Kamm, R. D. & Shapiro, A. H. 1979 Unsteady flow in a collapsible tube subjected to external pressure or body forces. *J. Fluid Mech.* **95**, 1–78.

Katz, A. I., Chen, Y. & Moreno, A. H. 1969 Flow through a collapsible tube. *Biophys. J.* **9**, 1261–1279.

Kececioglu, I., McClurken, M. E., Kamm, R. D. & Shapiro, A. H. 1981 Steady, supercritical flow in collapsible tubes. Part I. Experimental observations. *J. Fluid Mech.* **109**, 367–389.

Lambert, R. K. & Wilson, T. A. 1972 Flow limitation in a collapsible tube. *J. Appl. Physiol.* **33**, 150–153.

Lyon, C. K., Scott, J. B., Anderson, D. K. & Wang, C. Y. 1981 Flow through collapsible tubes at high Reynolds numbers. *Circulation Res.* **49**, 988–996.

McClurken, M. E., Kececioglu, I., Kamm, R. D. & Shapiro, A. H. 1981 Steady, supercritical flow in collapsible tubes. Part 2. Theoretical studies. *J. Fluid Mech.* **109**, 391–415.

Pedley, T. J. 1980 *The Fluid Mechanics of Large Blood Vessels.* Cambridge University Press.

Reyn, J. W. 1974 On the mechanism of self-excited oscillations in the flow through collapsible tubes. *Delft Progr. Rep., Ser. F* **1**, 51–67.

ROACHE, P. J. 1972 *Computational Fluid Dynamics*. Albuquerque, NM: Hermosa.

ROUSE, H. (ed.) 1950 *Engineering Hydraulics*. Wiley.

SCHLICHTING, H. 1968 *Boundary Layer Theory* (6th edn). McGraw-Hill.

SCHOENDORFER, D. W. & SHAPIRO, A. H. 1977 The collapsible tube as a prosthetic vocal source. *Proc. San Diego Biomed. Symp.* **16**, 349–356.

SHAPIRO, A. H. 1977*a* Physiologic and medical aspects of flow in collapsible tubes. *Proc. 6th Canadian Congr. Appl. Mech.*, pp. 883–906.

SHAPIRO, A. H. 1977*b* Steady flow in collapsible tubes. *Trans. ASME* K: *J. Biomech. Engng* **99**, 126–147.

SHIMIZU, M. & TANIDA, Y. 1983 On the mechanism of Korotkoff sound generation at diastole. *J. Fluid Mech.* **127**, 315–339.

UR, A. & GORDON, M. 1970 Origin of Korotkoff sounds. *Am. J. Physiol.* **218**, 524–529.

WILD, R., PEDLEY, T. J. & RILEY, D. S. 1977 Viscous flow in collapsible tubes of slowly varying elliptical cross-section. *J. Fluid Mech.* **81**, 273–294.